Pergamon

Geochimica et Cosmochimica Acta, Vol. 66, No. 20, pp. 3585–3598, 2002

0016-7037/02 $22.00 + .00

PII S0016-7037(02)00954-7

Sr and Nd isotope composition of Late Pleistocene sapropels and nonsapropelic sediments from the Eastern Mediterranean Sea: Implications for detrital influx and climatic conditions in the source areas

SYEE WELDEAB,[a,b,*] KAY-CHRISTIAN EMEIS,[b] CHRISTOPH HEMLEBEN,[a] TORSTEN W. VENNEMANN,[c] and HARTMUT SCHULZ[b]

[a]Institut und Museum für Geologie and Paläontologie, Universität Tübingen, Tübingen, Germany
[b]Institut für Ostseeforschung Warnemünde, Warnenünde, Germany
[c]Institut für Mineralogie, Petrologie und Geochemie, Universität Tübingen, Tübingen, Germany

(*Received February* 8, 2001; *accepted in revised form May* 29, 2002)

Abstract—Isotopic ratios of Sr and Nd from lithogenic components of three isochronous core sections recovered from an east–west transect in the Eastern Mediterranean Sea (EMS) have been analyzed. The data are used for a quantitative estimate of the temporal and spatial variation of detrital flux to the EMS, assuming Saharan dust and Aegean/Nile particulate matter as dominant end members. It was established that the carbonate-free Saharan dust flux during deposition of the nonsapropel layers of marine oxygen isotope stage 5.4 (MIS 5.4) was similar to the present flux. During the deposition of sapropels S5 and S6, however, the Saharan dust input was drastically reduced and was not balanced by a change in the riverine influx at this time. Denser vegetation cover during more humid conditions may have reduced physical erosion and sediment removal in the source area. During marine oxygen isotope stage 6.2 (MIS 6.2) a pronounced increase of Saharan dust and detrital influx from the Aegean region is evident and implies more arid conditions in the southern and northern catchment areas. During this period, intersite variations are interpreted in terms of their geographic location relative to the seaways connecting the Aegean Sea and EMS. The width of the straits and hence the amount of sediment entering the eastern basins may have been affected by a low sea level that impeded interbasin sediment dispersal. *Copyright © 2002 Elsevier Science Ltd*

1. INTRODUCTION

Sedimentary sequences from the eastern basin of the Mediterranean Sea and aerially exposed sections of Neogene age in southern Italy, Sicily, and Crete contain a series of sapropel layers (cm to m thick) sandwiched between hemipelagic, carbonate-rich sediments deposited under oxic conditions. The sapropels are rich in organic carbon and were deposited during periods when the deep waters of the eastern basins were oxygen depleted (Olausson, 1961; Kidd et al., 1978; Emeis et al., 2000). Low oxygen content in the eastern basins was probably preceded by the establishment of a density stratification of the water column and by enhanced productivity (Rossignol-Strick et al., 1982; Rohling and Gieskes, 1989). This requires an increased input of freshwater (Rossignol-Strick et al., 1982). The geographic origin of the increased freshwater influx has not been identified yet. A review and summary of existing models proposed for sapropel genesis has been presented by Cramp and O'Sullivan (1999).

The mineralogical and chemical composition of sapropel-containing sedimentary cycles indicates that changes in the source of detrital matter vary cyclically between eolian and riverine end members (Foucault and Mèlières, 2000; Wehausen and Brumsack, 2000). The chemical and mineralogical characteristics permit a differentiation between materials originating from different locations in the Eastern Mediterranean catchment area. Aluminum-normalized element ratios, according to Wehausen and Brumsack (2000) and Calvert and Fontugne (2001) indicate rhythmic alternations of eolian and fluvial input that are related to precession-induced climatic variations. A similar pattern of rhythmic changes for the origin of detrital material has been observed from clay-mineral analyses (Foucault and Mèlières, 2000). Characteristic chemical compositions (low K and Mg content) and mineral assemblages (high smectite content), indicative of the Nile provenance, are pronounced for sapropel members in the central and eastern part of the Levantine Basin, whereas the intervening nonsapropel sediments mainly contain material characteristic of modern Saharan and Damascus dust—that is, material blown in from the eastern borderland of the Eastern Mediterranean Sea (EMS; high Ti, Zr, palygorskite, and kaolinite content). In the westernmost Levantine and Ionian basins, the eolian end member is also dominated by sediments of Saharan origin; the composition of detrital matter of riverine origin is consistent with a source in the northern watershed of the EMS (high K, Mg, smectite, and chlorite contents). The latter is pronounced during insolation maxima and sapropel formation (Dominik and Stoffers, 1978; Foucault and Mèlières, 2000).

Strontium and neodymium isotopes have been successfully applied to characterize sediment provenance and reconstruct atmospheric and temporal variation of sediment supply to basins (e.g., Dia et al., 1992; Grousset et al., 1992; Revel et al., 1996; Asahara et al., 1999; Krom et al., 1999a, b). The reason for their extensive use is that their isotope ratios bear a fingerprint of their source rocks. Although the Nd isotope composition is little affected by grain-size differences of the sediment fractions and also robust to changes during weathering, transport, and winnowing processes (Goldstein et el., 1984; Walter et al., 2000), the Sr isotope composition can be influenced by

* Author to whom correspondence should be addressed, at Fachbereich Geowissenschaften, Universität Bremen, Postfach 330 440 28334 Bremen Germany (sweldeab@uni-bremen.de).

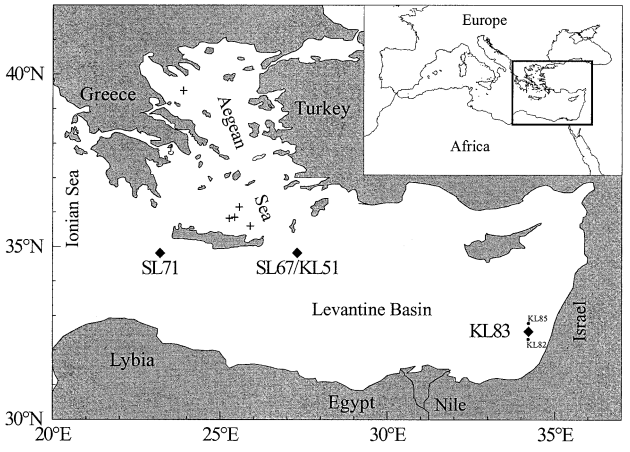

Fig. 1. Map of the Eastern Mediterranean Sea and core locations investigated in this study. Location of surface sediment samples in the Aegean Sea are also shown (+).

grain-sized sorting as well as during diagenesis of the sediment (Dasch, 1969; Walter et al., 2000). Nevertheless, Sr and Nd isotope compositions provide additional indicators for paleoenvironmental changes and identification of detrital sediment sources along with the bulk chemistry and clay mineralogy of the sediment (Foucault and Mèlières, 2000; Wehausen and Brumsack, 2000).

Quantitative reconstructions of the temporal and spatial variations of the terrigenous fractions track erosional processes and the dominant modes of transport and hence can be used to interpret the climatic conditions in the source areas. Climate, in turn, influences the hydrology and sedimentation budget of a semienclosed basin such as the eastern Mediterranean basin. The objectives of this study are to characterize and quantify the dominant provenance and mode of transport of the lithogenic sediments during different climatic conditions (interglacial, glacial) and during sapropel formation in the catchment of the EMS. By comparing different time slices, it is possible to constrain the conditions triggering and accompanying sapropel formation.

The Sr and Nd isotope composition of the lithogenic fraction of isochronous sediments in three sediment cores have been studied. The cores were specifically selected to trace dominant pathways of riverine material input to the EMS (Fig. 1). Surface sediments, sapropel 5 (S5), sapropel 6 (S6) as well as nonsapropel sediments above and beneath the sapropels were investigated. The two sapropels are distinct because S5 was deposited during the Eemian warm phase (starting 127 kyr ago) and S6 formed during the fully glacial phase of MIS 6 (starting 176 kyr ago). The two sapropels and intervening sediments thus bracket the entire range of environmental and climatic conditions in the EMS catchment during the Late Pleistocene. In light of the isotopic fingerprints, the diagnostic capability of chemical composition of bulk sediments as a tracer of terrigenous provenance can be evaluated.

2. MATERIALS AND METHODS

2.1. Sampling

Gravity cores SL71 (station 71, 34°48.61 N/23°11.66 E; water depth, 2827 m), SL67 (station 67, 34°48.83 N/27°17.77 E; water depth: 2157 m), piston cores KL51 (the same position and water depth as SL67) and KL83 (station 213, 32°36.87 N/34°08.89; water depth, 1431 m) were recovered during R/V *Meteor* expeditions M40/4 (spring 1998) and M44/3 (spring 1999). Core locations are shown in Fig. 1. Two parallel subsamples were taken from the cores for inorganic geochemistry and stable isotope analysis with syringes with a volume of 10 mL at a sample spacing of 2 cm. After determining volume and wet weight of the subsamples, they were oven dried at 105°C for 48 h; their weight loss was determined, and dry bulk density (g/cm^3) was calculated as ratio of dry weight/wet volume of the sample.

2.2. Analytical Procedures

For radiogenic isotope analysis of the detrital fractions, 500 mg of powdered and homogenized sediment were leached with 10 mL acetic acid (5 mol/L) at room temperature for 12 h. The detrital residue was rinsed four times with deionized water and centrifuged. Afterward the water was pipetted off. Previous work (Freydier et al., 2001) demonstrated the efficiency of the applied leaching method to remove the carbonate fraction of the samples. A total of 50 mg of the dried residue were spiked with a mixed ^{149}Sm:^{150}Nd spike before digestion in HF. The digested samples were dried and dissolved in 6 N HCl, dried, and then redissolved in 2.5 N HCl. For isotope analyses, Sr and light rare earth elements were isolated on quartz columns by conventional ion exchange chromatography with a 5-mL resin bed of Bio-Rad AG 50W-X12, 200 to 400 mesh. Nd was separated from other rare earth elements on quartz columns with 1.7-mL Teflon powder coated with HDEHP, di(2-ethylhexyl)orthophosphoric acid, as cation exchange medium. The ^{87}Sr/^{86}Sr and ^{143}Nd/^{144}Nd ratios were measured on a Finnigan MAT 262 mass spectrometer in static collection mode at the Institute for Mineralogy, Petrology, and Geochemistry, University of Tübingen. Analyses of NBS-SRM 987 and Nd Ames-Metal measurements while this study was being conducted yielded ^{87}Sr/^{86}Sr = 0.710236 ± 16 (2σ, n = 4) and ^{143}Nd/^{144}Nd = 0.512124 ± 14 (2σ, n = 4), respectively. On the basis of the small number of standards and adjusting the error by Student's *t* test yields estimated errors of 51 and 49 for Sr and Nd isotope ratios, respectively. ^{87}Sr/^{86}Sr ratios are normalized to ^{86}Sr/^{88}Sr = 0.1194 and ^{143}Nd/^{144}Nd ratios to ^{146}Nd/^{144}Nd = 0.7219. Measurement of the La Jolla Nd standard in our laboratory over a much longer period yielded 0.511850 ± 10 (n = 25). ^{143}Nd/^{144}Nd ratios are expressed as $\varepsilon_{Nd}(0)$, where $\varepsilon_{Nd}(0)$ are isotopic values normalized to the "chondritic uniform reservoir" value (0.512636) of Jacobson and Wasserburg (1980).

Oxygen isotope ratios of calcitic foraminiferal tests were analyzed to establish the stratigraphic position of sediment intervals sampled. Between 10 and 17 tests of planktic foraminifer *Globigerina ruber* (white) were picked from the size fraction >250 μm and ultrasonically cleaned. The samples were reacted at 90°C with 100% orthophosphoric acid on an automated carbonate device (Kiel-device) linked to a Finnigan MAT 251 mass spectrometer whose reference gas was calibrated with NBS 19, NBS 20, and NBS 28. The results are reported in the conventional per mil notation with reference to Vienna Pee Dee Belemnite. The external reproducibility for stable oxygen isotopes is better than 0.03‰. The measurements were conducted at the Leibniz Laboratory for Radiometric Dating and Stable Isotope Research, University of Kiel. The age models for the cores are based on a graphic correlation of the curves for δ^{18}O values with the SPECMAP isotope curve of Martinson et al. (1987) by the software package AnalySeries (Paillard et al., 1996). Linear sedimentation rates were assumed between the fixed isotope boundaries. The onset and cessation of sapropel formation were determined by noticeable increase and decrease of the barium content, respectively.

The total terrigenous burial flux has been calculated for each core as the product of the fractional weight percent of the detrital components [100 − ($CaCO_3$[wt%] + OM [wt%])], dry bulk density (g/cm^3), and sedimentation rate (cm/kyr). Organic matter (OM) content is obtained by multiplying the total organic carbon content with a theoretically derived factor 2.5. Authigenic minerals such as clay minerals, anhydrite, and Mn and Fe oxides are difficult to distinguish from detrital minerals. Given that the terrigenous flux is relatively high, the fraction of authigenic minerals is probably very low. In the sapropel layers, "biogenic barite" content, as recalculated from "biogenic" barium, is high. The highest value, however, is below 0.25 wt% of the total

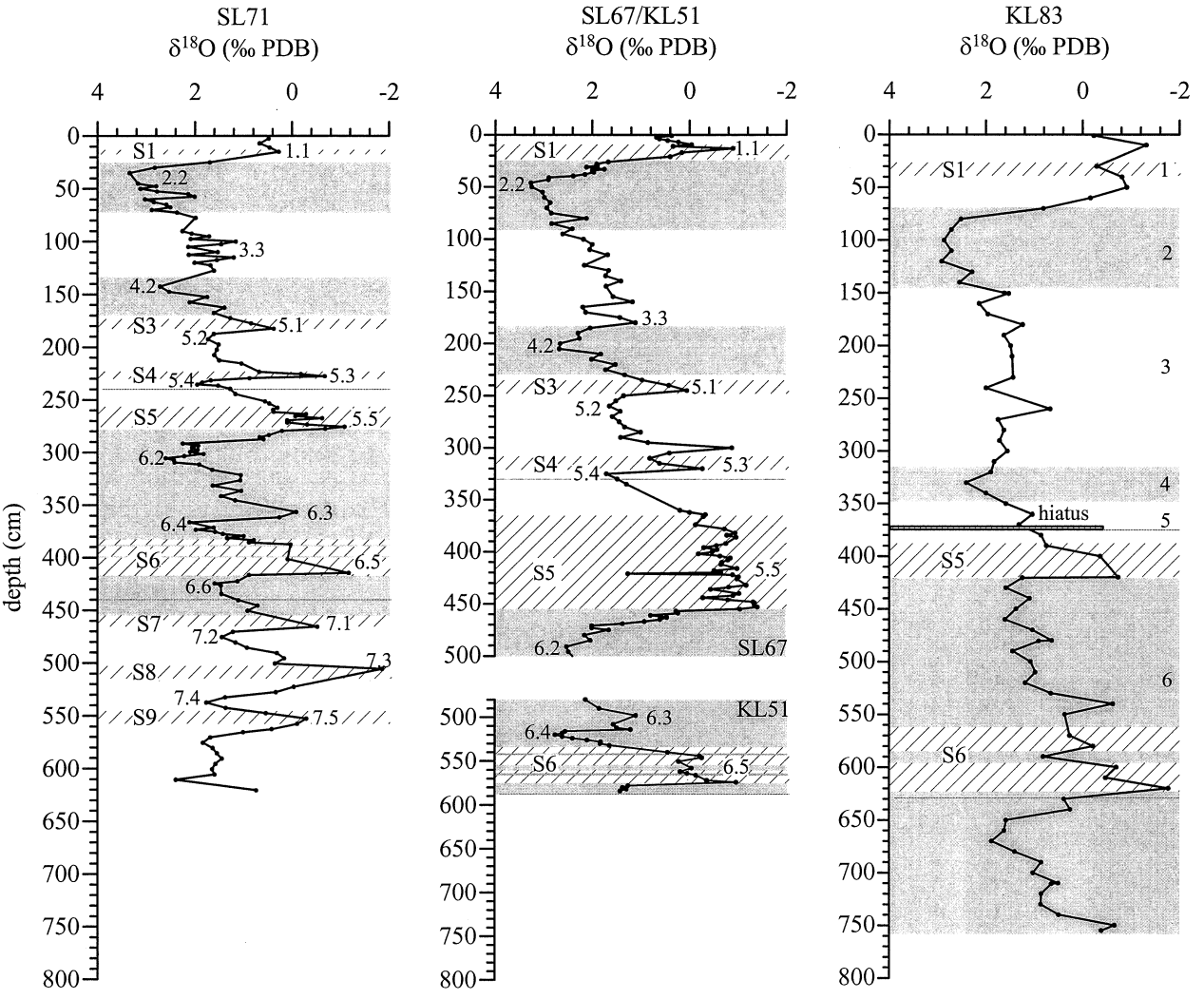

Fig. 2. Stable oxygen isotope composition of *Globigerina ruber* vs. depth in SL71, SL67/KL51, and KL83. Isotope stages (numbers), glacial phases (gray), and sapropels (striped) are indicated. Horizontal lines show investigated core sections. Note that the curve for SL67/KL51 consists of two core sections.

sediment. Biogenic opal is absent in the nonsapropelic sediments as a result of the oligotrophic conditions and dissolution in the sapropelic sediments (Kemp et al., 1998). Thus, biogenic opal has not been considered in the calculation.

3. RESULTS

3.1. Stratigraphy

Records of $\delta^{18}O$ values of investigated cores mirror the standard isotope curve (e.g., Martinson et al., 1987). However, the glacial–interglacial changes are much more pronounced and $\delta^{18}O$ values of calcareous foraminiferal tests during deposition of sapropels are extremely low (Fig. 2 and Table 1). In addition to the $\delta^{18}O$ values, ash layers and the typical interruption of S6 were used for inter and intracore comparisons. In KL83, we note that the sediment interval representing isotope stages 5.2 to 5.4 are missing because of a hiatus. The base of the hiatus is 13 cm above S5. SL67 did not penetrate down to sapropel 6, but parallel core KL51 did.

3.2. Sr and Nd Isotope Compositions

The results of Sr and Nd isotope analyses and calculated $\varepsilon_{Nd}(0)$ values are summarized in Table 2. In core SL71, the surface sediment $^{87}Sr/^{86}Sr$ ratio and $\varepsilon_{Nd}(0)$ value are within the range of those from MIS 5.4, which have average values for $^{87}Sr/^{86}Sr = 0.716$ and $\varepsilon_{Nd}(0) = -11$ (Fig. 3). S5 is marked by the lowest $^{87}Sr/^{86}Sr$ ratios and highest $\varepsilon_{Nd}(0)$ values ranging between 0.710 to 0.712 and -7.6 to -8.7, respectively. Data from MIS 6.2 plot within a narrow range and have a mean $^{87}Sr/^{86}Sr$ of 0.715 and $\varepsilon_{Nd}(0) = -10$ (Fig. 3). Compared with the nonsapropel MIS 6.2 samples, samples from S6 have lower $^{87}Sr/^{86}Sr$ and higher $\varepsilon_{Nd}(0)$ values and show more scatter. Comparison of the four sample sets from this location indicates an increase of $\varepsilon_{Nd}(0)$ values and decrease of $^{87}Sr/^{86}Sr$ ratios from MIS 5.4 to MIS 6.2, S6, and to S5. The $^{87}Sr/^{86}Sr$ ratios and $\varepsilon_{Nd}(0)$ values plot very close to the calculated mixing hyperbola between the data for Saharan dust and Aegean-Nile sediments (Fig. 3). In core SL67, surface sediment ($^{87}Sr/^{86}Sr =$

Table 1. $\delta^{18}O$ values of planktic foraminiferal tests (*Globigerinoides ruber* var. white) of investigated cores.

SL71 (cm)	$\delta^{18}O$ (‰)	SL67 (cm)	$\delta^{18}O$ (‰)	KL51 (cm)	$\delta^{18}O$ (‰)	KL83 (cm)	$\delta^{18}O$ (‰)	SL71 (cm)	$\delta^{18}O$ (‰)	SL67 (cm)	$\delta^{18}O$ (‰)	KL83 (cm)	$\delta^{18}O$ (‰)	SL71 (cm)	$\delta^{18}O$ (‰)	SL67 (cm)	$\delta^{18}O$ (‰)	KL83 (cm)	$\delta^{18}O$ (‰)	SL71 (cm)	$\delta^{18}O$ (‰)	SL67 (cm)	$\delta^{18}O$ (‰)
3	0.5	1	0.37	460	3.72	1	−0.2	143	2.72	100	2.18	360	1.04	270	0.09	280	1.33	690	0.86	496	0.15	426	−1
7	0.7	3	0.68	470	3.74	10	−1.3	148	2.53	105	2	370	1.32	272	0.09	285	1	700	1.03	501	0.34	428	−0.3
11	0.5	4	0.62	480	2.98	30	−0.3	153	1.75	110	2.05	380	0.86	274	−0.3	290	1.41	710	0.51	506	−1.9	432	−1.2
15	0.3	6	0.45	490	2.7	40	−0.8	158	2.11	115	1.68	390	0.75	276	−1.1	295	0.85	711	0.65	523	−0.1	434	−0.8
25	1.7	7	0.23	498	1.95	50	−0.9	163	1.39	125	2.16	400	−0.4	278	−0.7	300	−0.9	720	0.86	528	0.32	436	−0.4
30	2.8	10	−0	508	2.41	60	−0.2	168	1.61	130	1.66	420	−0.7	280	0.2	305	0.41	730	0.87	533	1.37	440	−1
35	3.3	11	0.34	512	2.34	70	0.81	173	1.27	135	1.72	421	1.25	284	0.47	310	0.81	740	0.5	538	1.76	442	−0.9
45	3.2	13	−0.9	514	2.06	80	2.52	178	0.84	140	1.41	430	1.59	286	0.66	315	0.61	750	−0.7	543	1.36	444	−0.3
48	2.8	15	−0	516	3.4	90	2.72	183	0.37	145	1.71	440	1.1	288	0.58	320	−0.3	755	−0.4	548	0.53	446	−0.8
50	3.1	17	0.16	518	3.46	100	2.87	188	1.61	155	1.57	450	1.38	292	2.25	325	1.7	SL71	$\delta^{18}O$	553	−0.3	448	−1.3
53	2.8	20	0.07	520	3.61	110	2.72	193	1.73	160	1.17	460	1.61	294	1.93	330	1.48	(cm)	(‰)	558	−0.1	449	−1.3
55	2.1	21	0.4	522	3.46	120	2.92	198	1.51	165	2.19	470	1.04	296	2.06	335	1.29	376	1.58	563	0.41	451	−1.3
58	2	26	1.67	524	3.25	130	2.29	203	1.55	170	2.13	480	0.64	298	1.94	350	0.18	378	1.42	566	1	453	−1.4
60	3	28	1.91	526	2.95	140	2.55	208	1.6	175	1.43	481	0.91	300	2.1	352	0.3	380	0.99	571	1.68	455	−1
63	2.9	30	1.89	528	2.67	150	1.62	213	1.5	180	1.11	490	1.45	302	1.82	354	0.19	382	1.33	576	1.83	457	0.27
65	2.6	31	2.12	530	2.68	151	1.53	216	1.04	185	2.04	500	1.08	304	2.22	356	0.51	384	0.78	581	1.63	459	0.23
68	2.5	33	1.75	532	2.49	160	2.14	224	0.67	190	2.29	510	0.98	306	2.6	358	−0.1	386	0.88	586	1.54	461	0.79
70	2.9	35	2	540	1.3	170	1.96	226	−0.2	195	2.26	520	1.19	308	2.43	360	0.19	388	0.02	591	1.44	463	0.46
73	2.4	36	1.97	544	0.65	180	1.24	228	−0.7	200	2.66	530	0.66	310	2.42	362	−0	402	0.08	596	1.57	465	0.6
78	2	38	2.15	546	0.6	190	1.63	230	0.87	205	2.68	540	−0.6	312	1.91	364	−0.3	415	−1.2	601	1.64	467	0.92
90	2.3	40	2.39	551	1.07	200	1.49	232	1.67	210	1.82	550	0.37	317	1.64	366	−0.3	417	0.88	606	1.59	469	1.37
93	2.1	41	2.9	558	0.81	210	1.46	234	1.85	215	2.01	560	0.35	322	1.05	374	−0.1	423	1.12	611	2.39	471	2
95	1.7	43	2.91	562	1.04	230	1.44	236	1.95	220	1.52	570	0.27	327	1.06	378	−0.7	425	1.59	621	0.73	473	2
98	2.1	46	3.27	564	0.9	240	2	237	1.52	225	1.72	580	−0.2	332	1.63	382	−0.9	427	1.46	SL67	$\delta^{18}O$	475	1.65
100	1.2	50	3.25	566	0.72	260	0.67	240	1.27	230	1.33	590	0.82	337	1.04	384	−0.8	435	1.45	(cm)	(‰)	480	2.15
103	1.5	55	3.03	572	0.5	270	1.75	245	1.16	235	0.97	600	−0.7	342	1.46	386	−1	441	1.1	408	−0.8	485	2.03
105	2.1	60	2.99	574	−0.1	280	1.63	252	0.55	240	0.42	610	−0.5	346	1.17	392	−0.8	446	0.7	410	−0.7	491	2.52
110	1.5	65	2.87	578	2.11	290	1.72	254	0.46	245	0.05	620	−1.8	347	−1.4	394	−0.6	451	0.91	412	−0.7	496	2.48
113	2.1	70	2.94	580	2.22	300	1.56	258	0.29	250	1.35	630	0.39	352	−0.6	396	−0.3	466	−0.5	416	−1	505	2.29
115	1.2	75	2.85	582	2.14	310	1.83	260	0.38	255	1.51	640	0.26	357	−0.1	398	−0.6	471	1.21	418	−0.5	510	2.23
118	1.6	80	2.12	584	2.27	320	1.9	262	0.37	260	1.64	650	1.59	362	0.25	400	−0.5	476	1.44	420	−0.7	515	1.84
120	2	85	2.84			330	2.41	264	−0.3	265	1.42	660	1.63	367	2.11	402	−0.2	481	1.16	421	1.26	520	1.84
123	1.7	90	2.41			340	2	266	−0.1	270	1.58	670	1.89	372	1.61	404	−0.6	486	0.92	422	−0.9	525	1.59
128	1.6	95	2.61			350	1.59	268	−0.6	275	1.44	680	1.41	374	1.98	406	−0.8	491	0.3	424	−1	530	0.93

Table 2. $^{87}Sr/^{86}Sr$ ratios, $^{143}Nd/^{144}Nd$ ratios, and $\varepsilon_{Nd}(0)$ values of all samples analyzed.

Core	Sediment type	Depth (cm)	$^{87}Sr/^{86}Sr$ ($\pm 2\sigma \times 10^{-6}$)	$^{143}Nd/^{144}Nd$ ($\pm 2\sigma \times 10^{-6}$)	$\varepsilon_{Nd}(0)$
SL71	Surface sediment	0–0.5	0.716950 (10)	0.512051 (10)	11.4
SL71	MIS 5.4	239.5	0.715731 (10)	0.512116 (10)	10.1
SL71	MIS 5.4	244.5	0.716351 (19)	0.512064 (10)	11.2
SL71	MIS 5.4	251.5	0.717411 (09)	0.512035 (10)	11.7
SL71	S5	263.5	0.710899 (17)	0.512243 (10)	7.7
SL71	S5	265.5	0.710770 (10)	0.512248 (09)	7.6
SL71	S5	269.5	0.711098 (10)	0.512224 (10)	8
SL71	S5	275.5	0.712378 (08)	0.512188 (10)	8.7
SL71	MIS 6.2	299.5	0.714715 (07)	0.512131 (10)	9.9
SL71	MIS 6.2	321.5	0.714920 (10)	0.512116 (10)	10.1
SL71	MIS 6.2	331.5	0.715607 (10)	0.512114 (11)	10.2
SL71	MIS 6.2	346.5	0.715369 (10)	0.512127 (10)	9.9
SL71	S6	387.5	0.711693 (10)	0.512247 (10)	7.6
SL71	S6	393.5	0.711750 (10)	0.512203 (10)	8.4
SL71	S6	401.5	0.712496 (08)	0.512176 (10)	9
SL71	S6	414.5	0.713281 (19)	0.512160 (10)	9.3
SL67	Surface sediment	0–0.5	0.714959 (10)	0.512152 (10)	−9.4
SL67	MIS 5.4	335.5	0.714126 (10)	0.512177 (10)	−9
SL67	MIS 5.4	341.5	0.714112 (10)	0.512146 (08)	−9.6
SL67	MIS 5.4	346.5	0.714568 (10)	0.512154 (08)	−9.4
SL67	MIS 5.4	350.5	0.714957 (10)	0.512119 (08)	−10.1
SL67	S5	386.5	0.710210 (11)	0.512251 (10)	−7.5
SL67	S5	400.5	0.710336 (10)	0.512253 (07)	−7.5
SL67	S5	416.5	0.710741 (10)	0.512255 (10)	−7.4
SL67	S5	446.5	0.710265 (10)	0.512258 (08)	−7.4
SL67	MIS 6.2	462.5	0.710672 (10)	0.512225 (10)	−8
SL67	Ash layer (MIS 6.2)	475.5	0.708284 (10)	0.512306 (09)	−6.4
KL51	MIS 6.2	470.5	0.711903 (10)	0.512234 (06)	−7.8
KL51	MIS 6.2	490.5	0.710921 (09)	0.512248 (07)	−7.6
KL51	S6	535.5	0.711860 (10)	0.512221 (10)	−8.1
KL51	S6	543.5	0.711011 (10)	0.512238 (10)	−7.8
KL51	S6	561.5	0.711783 (10)	0.512240 (08)	−7.7
KL51	S6	573.5	0.711896 (10)	0.512208 (08)	−8.3
KL82	Surface sediment	0–0.5	0.709053 (10)	0.512495 (08)	−2.8
KL85	Surface sediment	0–0.5	0.709381 (10)	0.512485 (10)	−2.9
KL83	Surface sediment	0–0.5	0.711353 (10)	0.512485 (08)	−2.9
KL83	S5	398	0.709344 (10)	0.512360 (09)	−5.4
KL83	S5	402	0.709322 (10)	0.512373 (08)	−5.1
KL83	S5	412	0.709291 (10)	0.512378 (08)	−5
KL83	S5	414	0.709275 (10)	0.512380 (08)	−5
KL83	MIS 6.2	460	0.708653 (10)	0.512433 (05)	−4
KL83	MIS 6.2	490	0.708684 (10)	0.512398 (07)	−4.6
KL83	MIS 6.2	510	0.709005 (10)	0.512399 (07)	−4.6
KL83	S6	566	0.709369 (10)	0.512406 (09)	−4.5
KL83	S6	572	0.709169 (10)	0.512407 (08)	−4.5
KL83	MIS 6.2	578	0.708831 (10)	0.512428 (08)	−4.1
KL83	S6	606	0.709092 (10)	0.512438 (08)	−3.9
KL83	S6	608	0.709008 (10)	0.512419 (10)	−4.2
KL83	S6	618	0.708949 (10)	0.512429 (07)	−4
MC515[a]	Aegan Sea surface sediment	0–0.5	0.713245 (10)	0.512247 (08)	−7.6
MC521[a]	Aegan Sea surface sediment	0–0.5	0.713724 (10)	0.512217 (09)	−8.2
MC522[a]	Aegan Sea surface sediment	0–0.5	0.713734 (10)	0.512206 (07)	−8.4
KL49[a]	Aegan Sea surface sediment	0–0.5	0.713831 (10)	0.512209 (10)	−8.4
KL50[a]	Aegan Sea surface sediment	0–0.5	0.710914 (10)	0.512341 (09)	−5.8

[a] Data from Weldeab et al. (2002).

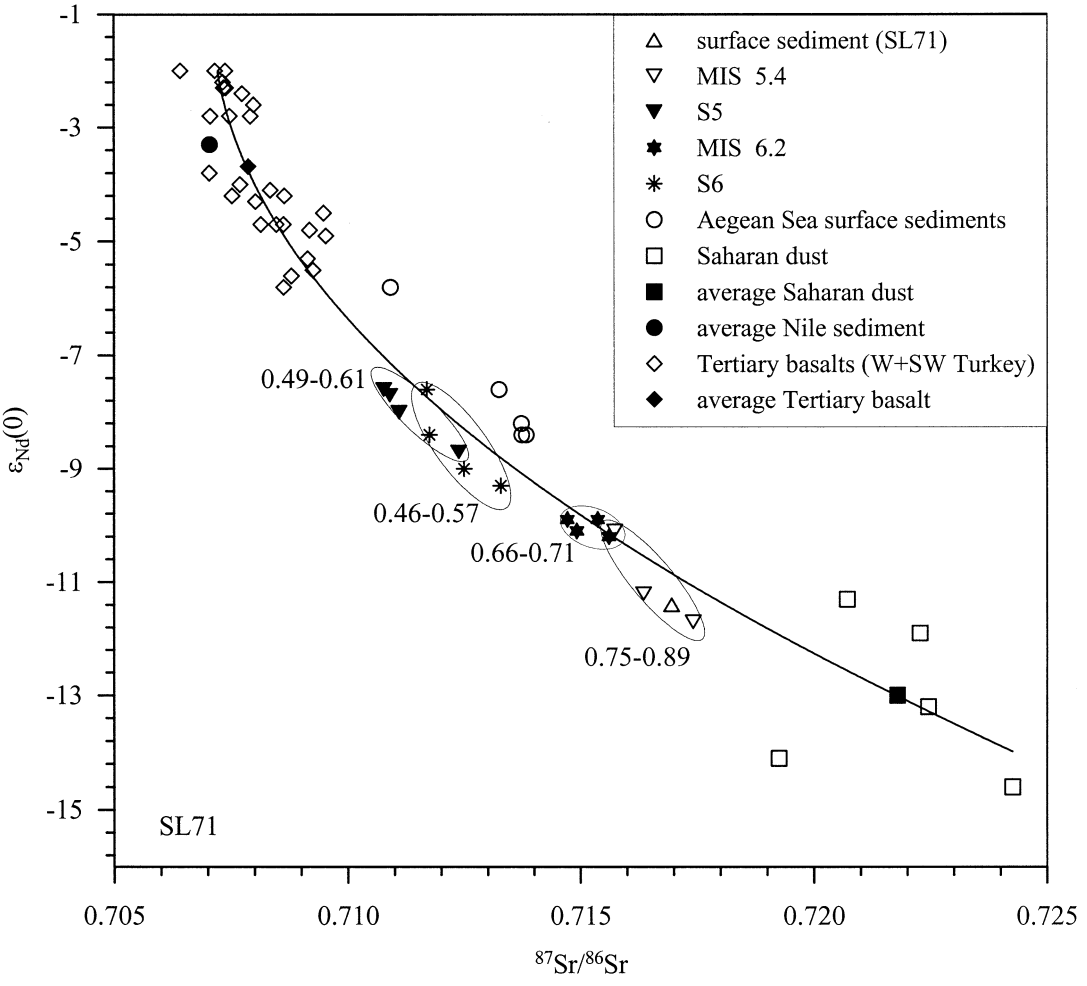

Fig. 3. $87Sr/^{86}Sr$ ratios vs. $^{147}Nd/^{144}Nd$ ratios (expressed as $\varepsilon_{Nd}(0)$) of lithic fraction of the samples in core SL71, potential source areas, and Aegean Sea lithogenic surface sediments. A calculated mixing line of the end members and the range of calculated Saharan dust fraction for the corresponding sediment is shown. Error bars are smaller than symbols. Data for Aegean Sea lithogenic surface sediments are from Weldeab et al. (2002); data for Saharan dust are from Grousset et al. (1998); data for Aegean basalts are from Güleç (1991); and data for Nile Delta sediment/particulate matter are from Goldstein et al. (1984) and Krom et al. (1999a).

0.714 and $\varepsilon_{Nd}(0) = -9.4$) and samples from MIS 5.4 have higher $^{87}Sr/^{86}Sr$ ratios (average = 0.714, n = 4) and lower $\varepsilon_{Nd}(0)$ values (average = −9.5, n = 4) compared with samples from S5 ($^{87}Sr/^{86}Sr$ ratios average = 0.710, n = 4; $\varepsilon_{Nd}(0)$ average = −7.4, n = 4) (Fig. 4). Samples from MIS 6.2 and S6 are similar and the means of $^{87}Sr/^{86}Sr = 0.711$ (n = 8) and $\varepsilon_{Nd}(0) = -7.7$ are close to those of S5 (Fig. 4). The surface sediments of core KL83 and those of cores KL82 and KL85 adjacent to KL83 (Fig. 1) are marked by highest $\varepsilon_{Nd}(0)$ values and moderate $^{87}Sr/^{86}Sr$ ratios having a mean of −2.9 and 0.710, respectively (Fig. 5). The samples of MIS 6.2 and S6 are not distinct with respect to their $^{87}Sr/^{86}Sr$ ratios and $\varepsilon_{Nd}(0)$ values (Table 2) and both have compositions similar to the Nile sediments. S5 differs from MIS 6.2 and S6 by having a slightly lower $\varepsilon_{Nd}(0)$ value (Fig. 5).

3.3. Terrigenous Burial Flux

During isotope stage MIS 5.4 the terrigenous flux of the site Southwest of Crete (SL71) is characterized by intermediate values with mean values of 2 g/cm^2/kyr (Fig. 6a). During S5 the total terrigenous flux was reduced to ~0.85 to 1 g/cm^2/kyr, whereas MIS 6.2 has the highest fluxes (average 5.2 g/cm^2/kyr). MIS 6.3 is marked by a terrigenous flux an order of magnitude lower and that is comparable to that of S5. An ash layer intercalated in MIS 6.3 is characterized by a higher value than the intervening sediments. An increased terrigenous flux (average values 2.4 g/cm^2/kyr) is evident during MIS 6.4. The lithogenic flux during deposition of S6 is low with 1 to 1.25 g/cm^2/kyr but slightly higher than that during S5.

The down core pattern of the terrigenous flux at the site southeast of Crete (SL67/KL51) is similar to that of SL71; however, the terrigenous flux is generally higher (Fig. 6a Average terrigenous flux at stage MIS 5.4 and during S5 accounts for 3.25 and 1.75 g/cm^2/kyr, respectively. In contrast to SL71, the transition between MIS 6.4 and S6 in SL67/KL51 is marked by a rather gradual increase of terrigenous flux. Furthermore, the decrease in the flux for S6 is not pronounced as for S6 of SL71. For KL83 the oxygen isotope stratigraphy yields no

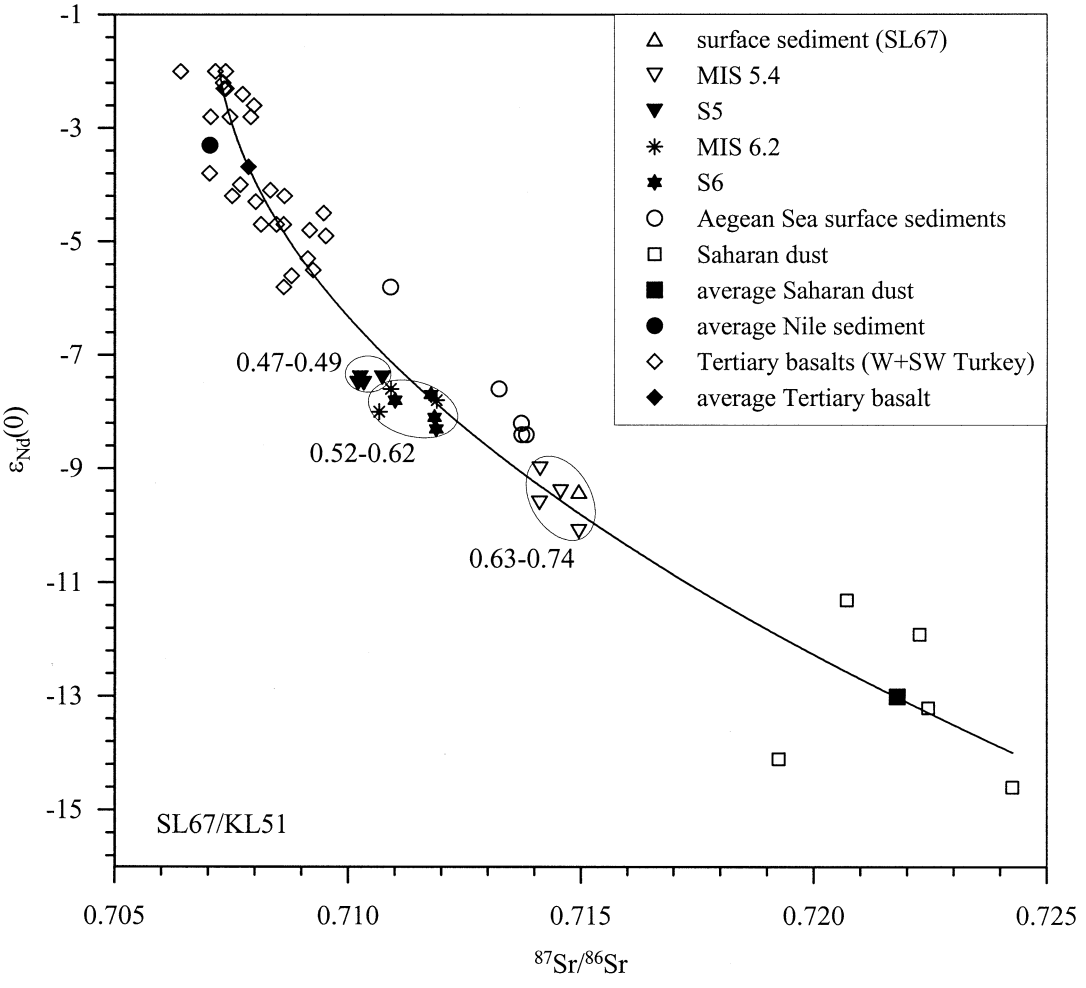

Fig. 4. $87Sr/^{86}Sr$ ratios plotted vs. $^{143}Nd/^{144}Nd$ ratios (expressed as $\varepsilon_{Nd}(0)$) of lithic fraction of the samples analyzed in cores SL67/KL51, potential source areas, and Aegean Sea lithogenic surface sediments. A calculated mixing line of the end members and the range of calculated Saharan dust fraction for the corresponding sediment is shown. Error bars are smaller than symbols. Data for the Aegean Sea lithogenic surface sediments and the potential source areas are taken from the literature as listed in the caption for Fig. 3.

unequivocal pattern because of a hiatus in this section. In addition, there are several microturbidites in the investigated core section. Because of those stratigraphic uncertainties, no flux calculations were made for this location.

4. DISCUSSION

4.1. Provenance, Mode of Transport, and Isotopic Characteristics of Modern Lithic Sediments in the EMS

The sedimentation of modern detritus to the EMS is dominated by Saharan dust and riverine particulate matter (Venkatarathnam and Ryan, 1971; Chester et al., 1977). The Saharan dust, which is sourced in the central and eastern parts of the North African desert (D'Almeida, 1986), is characterized by high $^{87}Sr/^{86}Sr$ ratios and low $\varepsilon_{Nd}(0)$ values (Grousset et al., 1998; Krom et al., 1999a). However, within the Mediterranean Sea, a slight east–west gradient in Sr isotope composition related to variations in the Saharan dust has been reported (Krom et al., 1999a). Eolian contributions from the eastern borderlands to the EMS are limited because of the prevailing southeast and northeast winds (Yaalon and Ganor, 1979; Ganor and Mamane, 1982; D'Almeida, 1989). In the central and eastern Levantine Basin, 97% of riverine-derived sediments are erosion products of the Atbara and Blue Nile catchment areas (Foucault and Stanley, 1989). These areas are made up of Tertiary basalts (Davidson and Rex, 1980). Thus, suspended Nile Delta sediments are characterized by low $^{87}Sr/^{86}Sr$ ratios (Krom et al., 1999a) and high $\varepsilon_{Nd}(0)$ values (Goldstein et al., 1984). These isotopic compositions are clearly reflected in the surface sediments of the central and eastern Levantine Basin (Weldeab et al., 2002). The present-day contribution of the White Nile accounts for 3% of total sediment loads transported by the Nile (Foucault and Stanley, 1989). Accordingly, the compositional influence of White Nile sediment loads on the Sr and Nd isotopes of the EMS sediments can be neglected. The

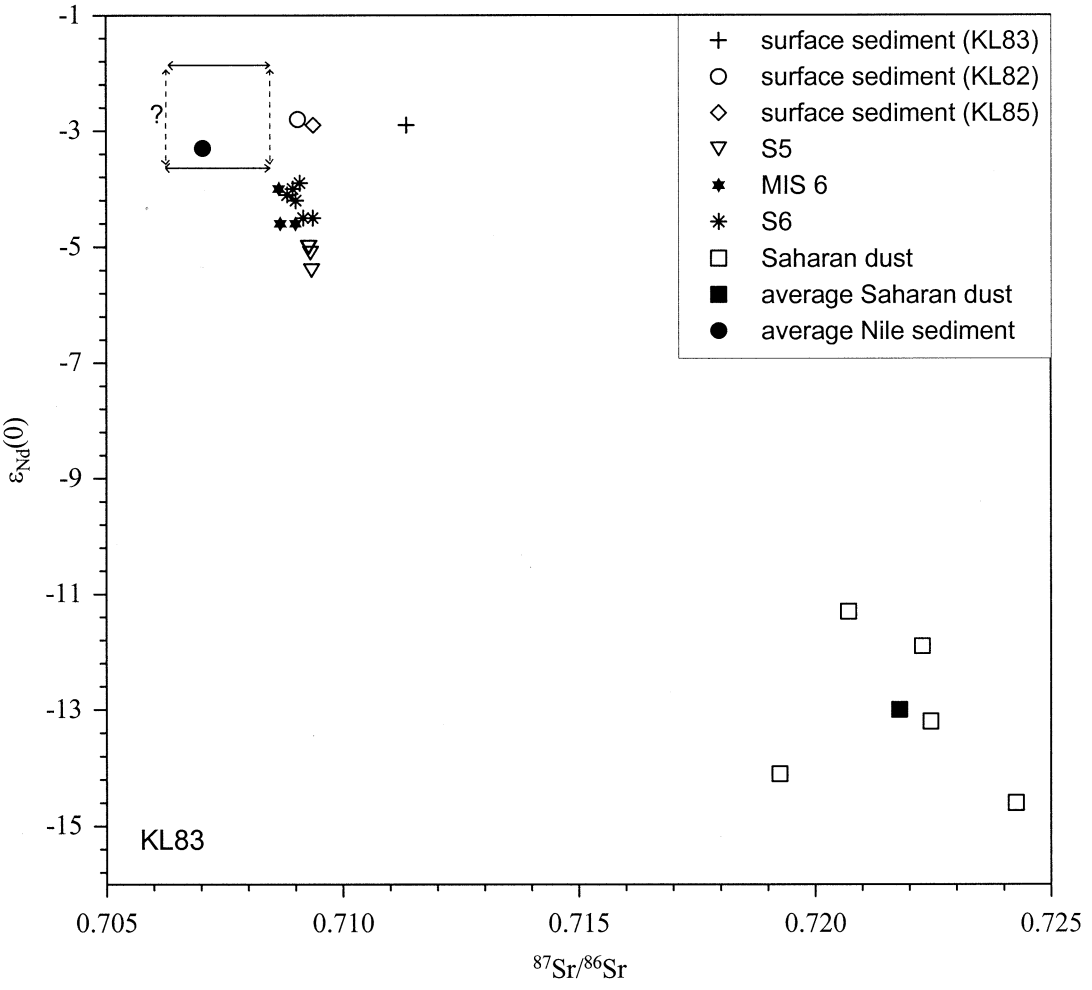

Fig. 5. $87Sr/^{86}Sr$ ratios and $^{143}Nd/^{144}Nd$ (expressed as $\varepsilon_{Nd}(0)$) of surface sediments from cores KL82, KL83, and KL85 as well as sapropels and homogeneous sediments from KL83 are shown. $^{87}Sr/^{86}Sr$ ratios and $\varepsilon_{Nd}(0)$ values of potential source areas are also displayed. Possible range of variability of the Nile sediments is shown by the box. Data for the source areas are taken from the literature as listed in the caption of Fig. 3.

role of ephemeral rivers from the Sinai and eastern borderlands to the EMS in supplying sediments is limited to the coastal area (Stanley et al., 1997, Stanley et al., 1998)

An important amount of riverine particulates are carried to the area south of Crete by the Levantine intermediate water from the Southeast, and by surface and deep water from the southwestern Aegean Sea (Venkatarathnam and Ryan, 1971; McCoy, 1974). Several rivers from southeastern Europe and western Turkey discharge into the Aegean. The catchment areas of the rivers draining western and southwestern Turkey as well as Greece are mainly composed of Oligocene to Quaternary basalts, ultramafic rocks, Cretaceous to Paleocene carbonates, and subordinate schists and granitic rocks (Fytikas et al., 1984c; Güleç, 1991; Voutsinou-Taliadouri and Varnavas, 1993). Available Sr and Nd isotope data of the Tertiary basalts (Güleç, 1991) from western and southwestern Turkey are very similar to those of the Nile Delta sediments. Nd and Sr isotope analyses of Aegean Sea lithogenic surface sediments point out that the suspended matter entering the Aegean Sea is characterized by high $\varepsilon_{Nd}(0)$ values and $^{87}Sr/^{86}Sr$ ratios (Weldeab et al in press). The $\varepsilon_{Nd}(0)$ values and $^{87}Sr/^{86}Sr$ do not plot exactly on but just next to the mixing line (Figs. 3, 4, and Table 2), indicating the influence of other minor sediment sources besides the assumed end members. Considering the diluting effect of the Saharan dust (high $^{87}Sr/^{86}Sr$ and low $^{143}Nd/^{144}Nd$ ratios), which is also a dominant sediment contributor to Aegean Sea (Pye, 1992), the detritus from the Aegean region entering the Aegean Sea must have higher $\varepsilon_{Nd}(0)$ values and lower $^{87}Sr/^{86}Sr$ ratios than those obtained for terrigenous surface sediments of the Aegean Sea (Weldeab et al., 2002) and would plot close to the Aegean end member. This supports our assumption that the basaltic and ultramafic rocks are dominant sources for detritus to the Aegean Sea and the EMS.

4.2. Dominant End Members of the Lithogenic Sediments in the EMS

Figures 3 to 5 display the Sr and Nd isotopic composition of the samples analyzed in this study. For SL67 and SL71, the $^{87}Sr/^{86}Sr$ and $^{143}Nd/^{144}Nd$ data plot on or close to a calculated

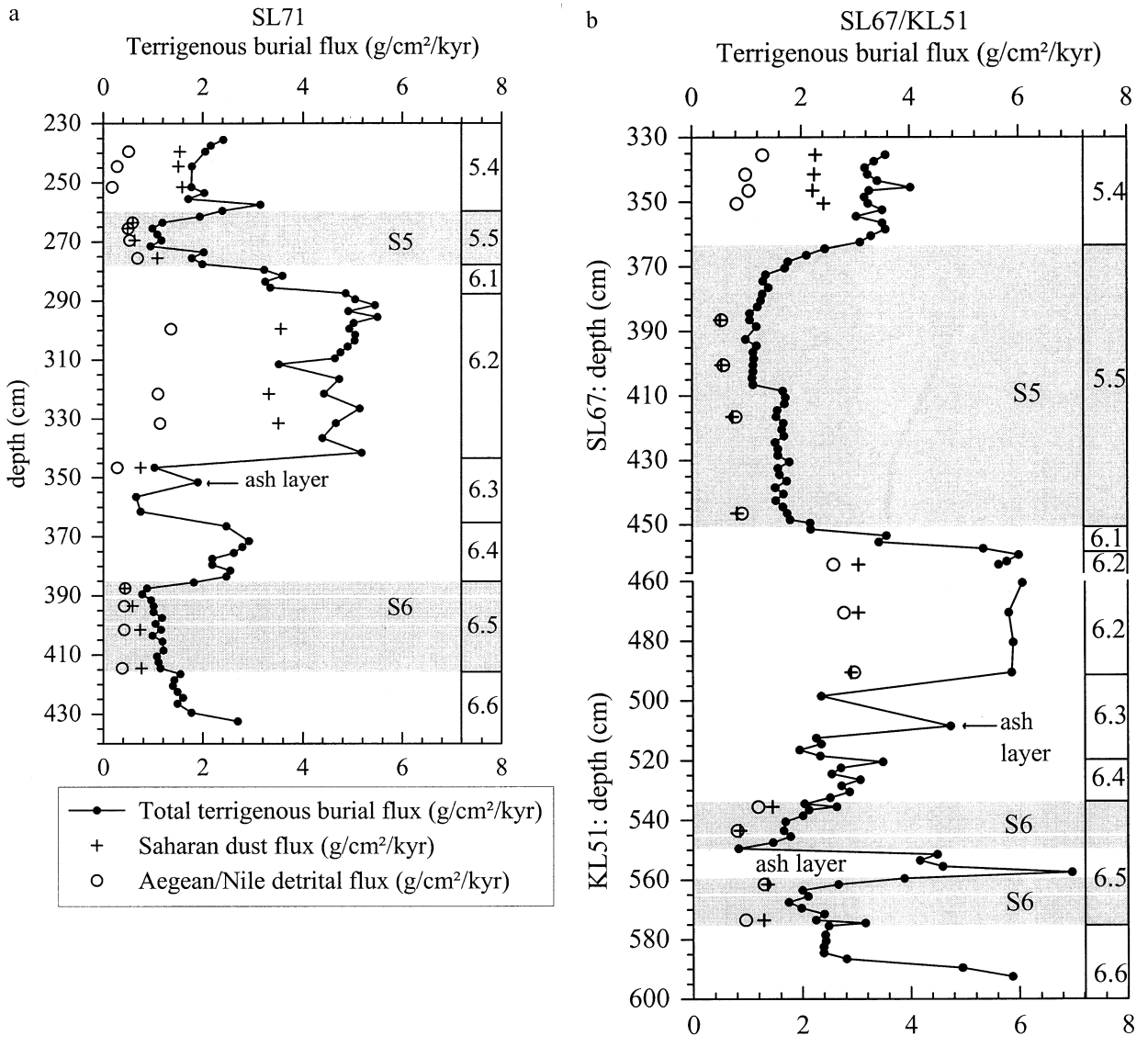

Fig. 6. Total terrigenous flux, Saharan dust flux, and Aegean/Nile sediment flux in SL71 (Fig. 6a) and SL67/KL51 (Fig. 6b) during deposition of the investigated sections.

hyperbolic mixing line, which assumes Saharan dust as one end member and Nile Delta sediments and/or Aegean basalts as the other (Figs. 3 and 4). This strongly supports the idea that the EMS detrital sediment fraction is mainly a mixture of Saharan dust and Nile or Aegean-derived detritus. Alternatively, it may be argued that the isotopic variation is associated with variability in circum-Aegean sediment sources without any significant effect from the Sahara. However, given that the drainage area (mostly northern Greece and western/southwestern Turkey) of the Aegean Sea is small and consists mostly of volcanic and ultramafic rocks (McCoy, 1974), the isotopic variation is likely to be small and would not explain the observed patterns. Contrary to this, the Saharan dust is a dominant sediment supplier to the EMS (Chester et al., 1977; Pye, 1992). Thus, variability in the amount of Saharan dust and/or input from the Aegean region would noticeably affect the isotopic composition of the EMS lithogenic sediment. Therefore, the present interpretation assumes that variations in the isotopic compositions through the investigated time interval are primarily caused by climate-coupled shifts in the proportion of Saharan dust and Aegean- or Nile-derived detritus entering the EMS. To prove the variability of source data, the $^{87}Sr/^{86}Sr$ ratios and $\varepsilon_{Nd}(0)$ values of Saharan dust (Grousset et al., 1998), Tertiary basalts from the western and southwestern Turkey (Güleç, 1991) assumed as representative of the Tertiary basalts in the Aegean region, and $^{87}Sr/^{86}Sr$ ratios (Krom et al., 1999a) and $\varepsilon_{Nd}(0)$ values of Nile particulate/delta sediments (Goldstein et al., 1984; Frost et al., 1986) have been plotted. For the Nile sediments, no coupled Sr and Nd isotope measurements on the same samples are available. However, the procedure is justified by the results of core KL83, which is rather close to the Nile Delta and is dominated by its fluvial input. The data of KL83 plot close to the combined data of Krom et al. (1999a), and Goldstein et al. (1984) and are tightly grouped (Fig. 5). We are

Table 3. Flux of total lithogenic matter, Saharan dust and Aegean/Nile detrial matter in the investigated core sections.

Depth (cm)	Total lithic flux (g/cm^2/kyr)	Saharan dust flux (g/cm^2/kyr)	Aegean/Nile flux (g/cm^2/kyr)	Depth (cm)	Total lithic flux	Saharan dust	Aegean/Nile flux	Depth (cm)	Total lithic flux	Saharan dust flux	Aegean/Nile flux
SL71											
235.5	2.4			311.5	3.5			416.5	1.6		
237.5	2.2			316.5	4.7			418.5	1.4		
239.5	2.0	1.5	0.5	321.5	4.4			420.5	1.4		
244.5	1.8	1.5	0.3	326.5	5.1			422.5	1.5		
251.5	1.8	1.6	0.2	331.5	4.7			424.5	1.6		
253.5	2.0			336.5	4.4			426.5	1.5		
255.5	1.7			341.5	5.2			429.5	1.8		
257.5	3.2			345.5	1.0	0.7	0.3	432.5	2.7		
259.5	2.4			351.5	1.9			434.5	1.8		
261.5	1.9			356.5	0.7			440.5	4.5		
263.5	1.2	0.6	0.6	361.5	0.8			445.5	4.3		
265.5	1.0	0.5	0.5	366.5	2.5			450.5	1.8		
267.5	1.1			371.5	2.9			455.5	1.3		
269.5	1.1	0.6	0.5	373.5	2.8			460.5	0.8		
271.5	1.0			375.5	2.6			465.5	0.9		
273.5	2.0			377.5	2.2			470.5	1.9		
275.5	1.8	1.1	0.7	379.5	2.2			475.5	1.3		
277.5	2.0			381.5	2.6			**SL67**			
279.5	3.2			383.5	2.5			335.5	3.6	2.3	1.3
281.5	3.6			385.5	1.8			337.5	3.4		
283.5	3.3			387.5	0.9			339.5	3.2		
285.5	3.4			389.5	0.8			341.5	3.2	2.2	1.0
287.5	4.9			391.5	1.0			343.5	3.4		
289.5	5.1			393.5	1.0	0.6	0.4	345.5	4.0		
291.5	5.5			395.5	1.0			346.5	3.3	2.2	1.0
293.5	4.9			397.5	1.2			348.5	3.2		
295.5	5.5			399.5	1.1			350.5	3.2	2.4	0.8
297.5	5.0			401.5	1.1	0.7	0.4	352.5	3.5		
299.5	4.9	3.5	1.4	403.5	1.0			354.5	3.0		
301.5	5.1			405.5	1.2			356.5	3.5		
303.5	5.0			408.5	1.2			358.5	3.6		
305.5	4.9			410.5	1.1			360.5	3.3		
307.5	4.8			412.5	1.1			362.5	3.1		
309.5	4.6			414.5	1.2	0.8	0.4	364.5	2.4		

also aware that the isotopic composition of the detrital components entering the EMS via the Aegean Sea does not only reflect that of the dominant rocks mentioned above (basaltic and ultramafic rocks), but also that of schists and granitic rocks. Thus, a wider range of the isotopic variability of the Aegean source area could be expected than shown by the data of Güleç (1991). However, the simple modeling presented below will assume that weathering products of the basaltic and ultramafic rocks dominate the isotopic compositions.

4.3. Model Calculation for Saharan Dust and Aegean/Nile Sediment Fluxes

For quantitative estimates of the relative amounts of sediment from the two assumed main source areas, the Saharan dust and the input from the Aegean and Nile, average Nd concentrations and isotopic ratios were taken from the literature: Nd = 28 ppm and $^{143}Nd/^{144}Nd = 0.511974$ ($\varepsilon_{Nd}(0) = -12.9$) for Saharan dust (Grousset et al., 1998) and $^{143}Nd/^{144}Nd = 0.512469$ ($\varepsilon_{Nd}(0) = -3.3$) for the Aegean region and Nile sediments (Goldstein et al., 1984; Güleç, 1991). The binary mixing equation developed by Faure (1986) was used for the calculation of fractional components of the two end members. By multiplying the fractional component of Saharan dust and Aegean/Nile components with the total terrigenous flux we obtain a quantitative estimate of contributions made up by the Saharan dust and Aegean/Nile input (Figs. 6a). Similar results were obtained by using average Sr concentrations and isotopic ratios for the two assumed main source areas from the literature: Sr = 115 ppm and $^{87}Sr/^{86}Sr = 0.7222$ for Saharan dust (Grousset et al., 1998) and Sr = 220 ppm and $^{87}Sr/^{86}Sr = 0.707$ for the Aegean region/Nile sediments (Krom et al., 1999a; Güleç, 1991). For MIS 6.2, the results obtained for Nd and Sr deviate somewhat, but the overall pattern remains similar. The present model results are based on Nd because of the lower sensitivity of this element to diagenetic effects.

4.4. Modern and Nonsapropel Sediments of Marine Isotope Stage 5.4 (MIS 5.4)

The isotopic composition of surface sediment and MIS 5.4 in SL67 and SL71 display the most unradiogenic values for Nd and most radiogenic for Sr, implying a predominance of sediment with Saharan origin. Because of the proximity to the Nile Delta, the isotopic composition of the surface sediment in KL83, and those of two cores (KL82 and KL85) adjacent to KL83, display highest $\varepsilon_{Nd}(0)$ values and are comparable to the "Pre–Aswan Dam" Nile sediments—that is, to sediments shed

Table 3. (continued)

Depth (cm)	Total lithic flux	Saharan dust flux	Aegean/Nile flux	Depth (cm)	Total lithic flux	Saharan dust flux	Aegean/Nile flux	Depth (cm)	Total lithic flux	Saharan dust flux	Aegean/Nile flux
						SL71					
366.5	2.1			436.5	1.7			528.5	2.7		
368.5	1.8			438.5	1.5			530.5	2.9		
370.5	1.7			440.5	1.7			532.5	2.5		
372.5	1.4			442.5	1.5			534.5	2.0		
374.5	1.3			444.5	1.7			535.5	2.6	1.5	1.1
376.5	1.4			446.5	1.7	0.8	0.9	536.5	2.1		
378.5	1.3			448.5	1.8			538.5	2.0		
380.5	1.3			449.5	2.2			540.5	1.7		
382.5	1.2			451.5	2.2			543.5	1.7	0.9	0.8
384.5	1.1			453.5	3.6			545.5	1.8		
386.5	1.0	0.5	0.5	455.5	3.4			547.5	1.5		
388.5	1.2			457.5	5.4			549.5	0.8		
392.5	1.0			459.5	6.0			551.5	4.5		
394.5	1.2			461.5	5.8			553.5	4.2		
396.5	1.1			462.5	5.6	3.0	2.6	555.5	4.6		
398.5	1.1			465.5	3.7			557.5	7.0		
400.5	1.1	0.5	0.6	467.5	3.4			559.5	3.9		
402.5	1.1			469.5	3.9			561.5	2.7	1.4	1.3
404.5	1.1			471.5	4.1			563.5	2.0		
406.5	1.1			**KL51**				565.5	2.1		
408.5	1.7			460.5	6.1			567.5	1.8		
410.5	1.7			470.5	5.8	3.0	2.8	569.5	2.0		
412.5	1.7			480.5	5.9			571.5	2.4		
414.5	1.6			490.5	5.9	2.9	3.0	573.5	2.3	1.3	1.0
416.5	1.5	0.7	0.8	498.5	2.4			574.5	3.2		
418.5	1.7			508.5	4.7			575.5	2.5		
420.5	1.6			512.5	2.3			578.5	2.4		
422.5	1.7			514.5	2.4			580.5	2.4		
424.5	1.5			516.5	2.0			582.5	2.4		
426.5	1.6			518.5	2.3			584.5	2.4		
428.5	1.6			520.5	3.5			586.5	2.8		
430.5	1.8			522.5	2.7			589.5	5.0		
432.5	1.6			524.5	2.5			592.5	5.9		
434.5	1.6			526.5	3.1						

prior the construction of the High Dam at Aswan (Egypt) in 1964 (Fig. 5). Calculated carbonate-free Saharan dust flux accounts for 1.5 to 1.6 g/cm^2/kyr in SL71 and 2.2 to 2.4 g/cm^2/kyr in SL67 (Table 3 and Figs. 6a, b). This is in good agreement with the present-day Saharan flux of 2 mg/cm^2/yr (=2 g/cm^2/kyr) and 1.52 mg/cm^2/yr (=1.52 g/cm^2/kyr) reported by Guerzoni et al. (1997) and Rutten et al. (2000), respectively. The similarity in isotopic composition and terrigenous flux between the surface sediment and those of MIS 5.4 suggests similar climatic conditions during MIS 5.4 compared with the present climate.

4.5. Sapropel S5 and the Eemian Warm Phase

The most significant change occurred during deposition of S5. The isotopic compositions are shifted to the most radiogenic values for Nd and unradiogenic for Sr (Figs. 3 and 4). In both SL67 and SL71 the total terrigenous flux was drastically reduced (Figs. 6a,b).

Compared with the surface sediments, S5 in KL83 is marked by slightly lower $\varepsilon_{Nd}(0)$ values and $^{87}Sr/^{86}Sr$. These climate-coupled variations of isotopic composition deviate from the patterns observed in SL67 and SL71 (Figs. 3 and 4). Hence, a third source may exist, which is possibly characterized by somewhat lower $\varepsilon_{Nd}(0)$ values than those of the Blue Nile sediments and also by lower $^{87}Sr/^{86}Sr$ ratios than Saharan dust. It could be speculated that an increased proportion of White Nile suspended matter and/or elevated sediment supply by ephemeral rivers draining the Sinai Peninsula and Israel may cause such a distinct change.

Our model calculations for SL71 and SL76/KL51 indicate that the shifts in Sr isotope ratios and $\varepsilon_{Nd}(0)$ values are caused by significant reduction of Saharan dust input, whereas there is little or no decrease in the riverine flux of the detritus (Figs. 6a,b). We conclude that the decrease of Saharan dust flux could be caused by enhanced humidity and northward migration of denser vegetation cover, reducing the dust ablation areas. This interpretation is supported by terrestrial (Petit-Maire, 1987) and paleontological records (Lèzine and Casanova, 1991) that point to a pluvial phase and a northward extension of phytogeographical zones and boundaries in North Africa during marine isotope stage 5.5, respectively. Evidence for a wet climate during sapropel formation is also provided by paleochannels (extinct river systems) draining the southeastern Sahara (Pachur and Kroepelin, 1989) and extended paleolakes in the North African desert (Gausse et al., 1989). Humid and wet climate that promoted the development of evergreen oak forest,

has also been recorded from the northern boundary of the eastern Mediterranean (NBEM) (Wijmstra and Witte, 1990; Cheddadi and Rossignol-Strick, 1995; Rossignol-Strick, 1999). The relationship between humid climate and low riverine detrital input as a consequence of the denser vegetation cover and, hence, reduced erosion/sediment removal in the catchment areas has been demonstrated by Foucault and Stanley (1989) and Hamroush and Stanley (1990) in the Nile Delta. Thus, a possible explanation for the more or less unchanged fluvial sediment input during the humid phases could be an increased vegetation cover that reduced the erosion and removal of sediment.

4.6. Glacial Nonsapropel Sediment: Temporal and Local Differences

The upper part of marine isotope stage 6 (MIS 6.2) is marked by the highest total terrigenous flux (Figs. 6a,b) In both SL67/KL51 and SL71, the $\varepsilon_{Nd}(0)$ and $^{87}Sr/^{86}Sr$ display intermediate values and lie between those of S5 and MIS 5.4 (Figs. 3 and 4). Both sites are characterized by increased fluxes of Saharan dust and "Aegean/Nile" material (Figs. 6a ,b) The contribution of detrital sediments with Aegean/Nile characteristics to the total lithic flux is approximately 27 to 28% in SL71 and 46 to 52% in SL67/KL51 (Figs. 3 and 4).

Aridity and enhanced wind strength may have increased the eolian contribution not only from the Saharan desert, but also from the Aegean region. However, local variation of eolian input as the only explanation for differences in the isotopic composition of Sr and Nd between the two sites (SL71 and SL67/Kl51) can be ruled out. An extension of the fluvial dispersal of sediments from the Nile toward the southeast of Crete and increased material input from southern Turkey could have resulted in site SL67/KL51 receiving more detrital matter with Aegean/Nile characteristics compared with site SL71. In addition, the bathymetry of the Strait of Kithira (between Peloponnesus and Crete) and the passage between the islands of Crete and Rhodes also has to be considered (Fig. 1). During glacials the sea level was lowered significantly. Considering the shallow bathymetry of the Aegean Sea and particularly that of the straits connecting the Aegean Sea with the EMS, the straits must have been narrower during sea level low stands. According to a bathymetric map for the last glacial (Thiede, 1978), the strait of Kithira was reduced to half its present width. This would have direct implications on the amount of water and suspended sediment that passed to areas southwest of Crete.

For MIS 6.3 in both SL71 and SL67/KL51 the total terrigenous input is similar to that during sapropel formation (Figs. 6a ,b) Apparently, environmental changes were not sufficient to trigger sapropel formation, but strong enough to induce noticeable reduction of terrigenous fluxes. Depletion of ^{18}O and enrichment of "biogenic" barium concentration also reveal hydrographic and productivity changes during this time interval (Weldeab et al., in press).

4.7. Sapropel 6 (S6)

By analogy to S5 and MIS 5.4, the isotopic compositions of S6 sediments from SL71 have more radiogenic $\varepsilon_{Nd}(0)$ values and lower $^{87}Sr/^{86}Sr$ ratios than MIS 6.2. Moreover, the data show significant variability (Fig. 3b). The total terrigenous burial flux for S6 is also reduced by an order of magnitude, which is similar to the reduction for S5 (Fig. 6a). On the basis of the isotopic data, the reduction in Saharan dust flux was not nearly as marked as that during deposition of S5, though (Figs. 3 and 6a). In SL67/KL51, the isotopic difference between S6 and MIS 6.2 is not pronounced. Both S6 and MIS 6.2 show Sr and Nd isotopic compositions that are close to those of S5 (Fig. 4). Compared with S6 in SL71, the reduction of the total terrigenous flux in SL67/KL51 is moderate suggesting that this site received more detrital matter with characteristics similar to that of the Aegean/Nile. In KL83, there is no noticeable difference in Sr and Nd isotopic composition between MIS 6.2 and S6 (Fig. 5), indicating a predominance of the Nile in supplying terrigenous sediments during these two different environmental conditions.

The Sr and Nd isotopic compositions and total lithogenic flux during S6 imply similar depositional condition as for S5 described above. Hence it can be argued that the processes during the deposition of S6 were similar, albeit less pronounced, than those discussed for S5.

5. CONCLUSIONS

Spatial and temporal variations of lithogenic components in sediments from the EMS have been reconstructed. The investigated sites and time slices allow to reconstruct dominant pathways of fluvial and eolian sediment input into the EMS and bracket the range of environmental and climatic conditions during the Late Pleistocene.

According to the isotopic composition of Sr and Nd, the terrigenous fraction in the easternmost part of the Levantine Basin is composed mainly of suspended particulate matter from the Nile and, to lesser extent, of the Saharan dust. Southeast and southwest of Crete, the eolian and fluvial contributions to the terrigenous flux are more or less balanced, and their climatically induced temporal variations are clearly reflected in the isotopic composition of the sediments.

Surface sediments and sediments of MIS 5.4 in core SL71 and SL67/KL51 are characterized by the highest $^{87}Sr/^{86}Sr$ ratios and lowest $\varepsilon_{Nd}(0)$ values. They reflect a predominant input of Saharan dust. This is consistent with a dominance of Saharan dust input to the lithogenic sedimentation during interglacial periods.

During deposition of S5, the total terrigenous flux was reduced by more than half when compared with nonsapropel sediments of MIS 5.4. The isotopic proxies indicate a significant reduction in Saharan dust flux but a more or less unchanged fluvial flux. A possible explanation for this observation is that a change toward a humid climate and a northward migration of denser vegetation implies reduced physical erosion and denudation of the southern catchment areas. S6 displays similar characteristics to S5, but the change is less pronounced. During deposition of S6, moderate humidity and less pronounced reduction of Saharan flux are indicated.

The glacial marine oxygen isotope stage 6.2 is characterized by the highest total terrigenous flux. The increased flux was caused by an elevated contribution of both "Aegean" (fluvial and eolian) and Saharan input. Glacial aridity and enhanced wind speeds caused a significant eolian contribution from the

north and northeast. The comparison between SL71 and SL67 suggests that the "Aegean/Nile" flux was higher southeast compared with southwest of Crete. A possible explanation for this difference in "Aegean/Nile" contribution could be an increased dispersal transport from south and southwest Turkey. Considering the location of the cores relative to the straits connecting the Aegean Sea with the EMS and the width and water depth of the straits, the Strait of Kithira may have been narrowed to half of its present width during stadial 6.2 (sea level low stand). As a result, less material would have reached the area southwest of Crete.

Acknowledgments—We thank the captain and crew of the R/V *Meteor* (cruises 40/4 and 44/3) for their help and assistance. U. Struck (University of Munich) is cordially thanked for his support during subsampling and hospitality during the stays of the first author in Warnemünde. We are indebted to R. Wehausen (University of Oldenburg) for critical reading and comments. We also thank E. Reitter for the Sr and Nd isotope analyses. Thoughtful and constructive reviews of Adina Paytan, Gareth Davies, an anonymous reviewer, and Steven L. Goldstein (AE) helped to substantially improve the manuscript. This work was funded by grants of the Deutsche Forschungsgemeinschaft to K.-C. Emeis (Em37/8) and Ch. Hemleben (He 697/28).

Associate editor: S. L. Goldstein

REFERENCES

Asahara Y. (1999) $^{87}Sr/^{86}Sr$ variation in North Pacific sediments: A record of the Milankovich cycle in the past 3 million years. *Earth Planet. Sci. Lett.* **171,** 453–464.

Calvert S. E. and Fontugne M. R. (2001) On the Late Pleistocene–Holocene sapropel record of climatic and oceanographic variability in the eastern Mediterranean. *Paleoceanography* **16,** 78–94.

Cheddadi R. and Rossignol-Strick M. (1995) Eastern Mediterranean Quaternary paleoclimates from the pollen and isotope records of marine cores in the Nile cone area. *Paleoceanography* **10,** 291–300.

Chester R., Baxter G. G., Behairy A. K. A., Nonnor K., Cross D., Elderfield H., and Padgham R. C. (1977) Soil-sized eolian dusts from the lower troposphere of the Eastern Mediterranean Sea. *Mar. Geol.* **24,** 201–217.

Cramp A. and O'Sullivan G. (1999) Neogene sapropels in the Mediterranean: A review. *Mar. Geol.* **153,** 11–28.

D'Almeida G. A. (1986) A model for Saharan dust transport. *J. Climate Appl. Meterol.* **25,** 903–916.

Dasch E. J. (1969) Strontium isotopes in weathering profiles, deep-sea sediments, and sedimentary rocks. *Geochim. Cosmochim. Acta* **33,** 1521–1552.

Davidson A. and Rex D. C. (1980) Age of volcanism and rifting in southwestern Ethiopia. *Nature* **283,** 657–658.

Dia A., Duprè B., and Allègere C. J. (1992) Nd isotopes in Indian sediments used as at tracer of supply to the ocean and circulation paths. *Mar. Geol.* **103,** 349–359.

Dominik J. and Stoffers P. (1978) The influence of Late Quaternary stagnations on clay sedimentation in the eastern Mediterranean Sea. *Geol. Rund.* **68,** 302–317.

Emeis K.-C., Sakamoto T., Wehausen R., and Brumsack H.-J. (2000) The sapropel record of the eastern Mediterranean Sea—Results of Ocean Drilling Program Leg 160. *Palaeoegeogr. Palaeoclimatol. Palaeoecol.* **158,** 371–395.

Faure G. (1986) *Principles of Isotope Geology*. Wiley.

Foucault A. and Stanley D. J. (1989) Late Quaternary palaeoclimaic oscillation in East Africa recorded by heavy minerals in the Nile Delta. *Nature* **339,** 44–46.

Foucault A. and Mèlières F. (2000) Palaeoclimatic cyclicity in central Mediterranean Pliocene sediments: The mineralogical signal. *Palaeoegeogr. Palaeoclimatol. Palaeoecol.* **158,** 311–323.

Freydier R., Michard A., De Lange G., and Thomson J. (2001) Nd isotopic compositions of Eastern Mediterranean sediments: Tracers of the Nile influence during sapropel S1 formation? *Mar. Geol.* **177,** 45–62.

Frost C. D., O'Nions R. K., and Goldstein S. L. (1986) Mass balance for Nd in the Mediterranean Sea. *Chem. Geol.* **55,** 45–50.

Fytikas M., Innocenti F., Manetti P., Mazzuoli Peccerillo A., and Villari L. (1984) Tertiary to Quaternary evolution of volcanism in the Aegean region. In *The Geological Evolution of the Eastern Mediterranean* (eds. J. E. Dixon and A. H. F Robertson), pp. 687–699. Blackwell.

Ganor E. and Mamane Y. (1982) Tranport of Saharan dust across the Eastern Mediterranean. *Atm. Environ.* **16,** 581–587.

Gausse C., Coque R., Fontes J. C., Gasse F., Gibert E., Ben Queodou H., and Zouari K. (1989) Two high levels of continental waters in the southern Tunisian chotts at about 90 and 150 ka. *Geology* **17,** 922–925.

Goldstein S. L., O'Nions R. K., and Hamilton P. J. (1984) A Sm-Nd isotopic study of atmospheric dusts and particulates from major river systems. *Earth Planet. Sci. Lett.* **70,** 221–236.

Grousset F. E., Rognon P., Coudè-Gaussen G., and Pèdemay P. (1992) Origins of peri-Saharan dust deposits traced by the their Nd and Sr isotopic composition. *Palaeoegeogr. Palaeoclimatol. Palaeoecol.* **93,** 203–212.

Grousset F. E., Parra M., Bory A., Martinez P. B. P., Shiemmield G., and Ellam R. M. (1998) Saharan wind regimes traced by the Sr-Nd isotopic composition of subtropical Atlantic sediments: Last Glacial maximum versus today. *Quat. Sci. Rev.* **17,** 395–409.

Guerzoni S., Molinaroli E., and Chester R. (1997) Saharan dust input to the western Mediterranean Sea: Depositional patterns, geochemistry and sedimentology implications. *Deep-Sea Res.* **44,** 631–654.

Güleç N. (1991) Crust-mantle interaction in western Turkey: Implications from Sr and Nd isotope Geochemistry of Tertiary and Quaternary volcanics. *Geol. Mag.* **128,** 417–435.

Hamroush H. A. and Stanley D. J. (1990) Paleoclimatic oscillations in East Africa interpreted by analysis of trace elements in Nile Delta sediments. *Episodes* **13,** 264–268.

Jacobson S. B. and Wasserburg G. J. (1980) Sm-Nd isotopic evolution of chondrites. *Earth Planet. Sci. Lett.* **50,** 139–155.

Kemp A. E. S., Pearce R. B., Pike J., and Marshall J. E. A. (1998) Microfabric and microcompositional studies of Pliocene and Quaternary sapropels from the Eastern Mediterranean Sea. *ODP Sci. Results* **160,** 333–342.

Kidd R. B., Cita M. B., and Ryan W. B. F. (1978) Stratigraphy of eastern Mediterranean sapropel sequences recovered during DSDP Leg 42A and their paleoenvironmental significance. *Init. Rep. DSDP* **42,** 421–443.

Krom M. D., Cliff R. A., Eijsink L. M., Herut B., and Chester R. (1999a) The characterisation of Saharan dusts and Nile particulate matter in surface sediments from the Levantine Basin using Sr isotopes. *Mar. Geol.* **155,** 319–330.

Krom M. D., Michard A., Cliff R. A., and Strohle K. (1999b) Source of sediment in the Ionian Sea and western Levantine Basin of the Eastern Mediterranean during S-1 sapropel times. *Mar. Geol.* **160,** 45–61.

Lèzine A.-M. and Casanova J. (1991) Correlated oceanic and continental records demonstrate past climate and hydrology of North Africa (0–140 ka). *Geology* **19,** 307–310.

Martinson D. G., Pisias N. G., Hays J. D., Imbrie J., Moore T. C., and Shackleton N. J. (1987) Age dating and the orbital theory of the Ice Age: Development of a high-resolution 0 to 300,000 year chronostratigraphy. *Quat. Res.* **27,** 1–29.

McCoy F. W. (1974) Late quarternary sedimentation in the Mediterranean Sea, Harvard University, Cambridge. pp. 132 (PhD thesis).

Olausson E. (1961) Studies in deep sea cores. *Deep Sea Expedition 1947–48,* **8,** 337–391.

Pachur H.-J. and Kroepelin S. (1989) Wadi Howar: Paleoclimatic evidence from an extinct river system in the southereastern Sahara. *Science* **237,** 298–300.

Paillard D., Labeyrie L., and Yiou P. (1996) Macintosh program performs time-series analysis. *EOS Trans. AGU* **77,** 379.

Petit-Maire N. (1987) Interglacial environments in presently hyperarid Sahara: Palaeoclimatic implications. *Paleoclimatology and Paleometeorology: Modern and Past Pattern of Global Atmospheric Transport* (eds. M. Leinen and M. Sarnthein), pp. 637–653. Kluwer.

Pye K. (1992) Eolian dust transport and deposition over Crete and adjacent parts of the Mediterranean Sea. *Earth Surf. Landforms* **17,** 271–288.

Revel M., Sinko J. A., and Grousset F. E. (1996) Sr and Nd isotopes as tracers of North Atlantic lithic particles: Paleoclimatic implications. *Paleoceanogrphy* **11,** 95–113.

Rohling E. J. and Gieskes W. W. C. (1989) Late Quaternary changes in Mediterranean intermediate water density and formation rate. *Paleoceanography* **4,** 531–545.

Rossignol-Strick M., Nesteroff W. D., Olive P., and Vergnaud-Grazzini C. (1982) After the deluge: Mediterranean stagnation and sapropel formation. *Nature* **295,** 105–110.

Rossignol-Strick M. and Paterne M. (1999) A synthetic pollen record of the eastern Mediterranean sapropels of the last 1 Ma: Implications for the time-scale and formation of sapropels. *Mar. Geol.* **153,** 221–237.

Rutten A., de Lange G. D., Ziveri P., Thomson J., van Santvoort P. J. M., Colley S., and Corselli C. (2000) Recent terrestrial and carbonate fluxes in the pelagic eastern Mediterranean; a comparison between sediment trap and surface sediment. *Palaeoegeogr. Palaeoclimatol. Palaeoecol.* **158,** 197–213.

Stanley D. J., Mart Y., and Nir Y. (1997) Clay mineral distributions to interpret Nile cell provenance and dispersal: II. Coastal plain from Nile Delta to northern Israel. *J. Coastal Res.* **13,** 506–533.

Stanley D. J., Nir Y., and Galili E. (1998) Clay mineral distributions to interpret Nile cell provenance and dispersal: III. Offshore margin between Nile and Northern Israel. *J. Coastal Res.* **14,** 196–217.

Thiede J. (1978) A glacial Mediterranean. *Nature* **276,** 680–683.

Venkatarathnam K. and Ryan W. B. F. (1971) Dispersal patterns of clay minerals in the sediments of the Eastern Mediterranean Sea. *Mar. Geol.* **11,** 261–282.

Voutsinou-Taliadouri F. and Varnavas S. P. (1993) Geochemical study of sediments from northern Euborkos Bay, Greece, with regard to the presence of submarine mineral deposits. *Mar. Geol.* **110,** 93–114.

Walter H. J., Hegner E., Diekamn B., Kuhn G., and Van der Loeff M. M. R. (2000) Provenance and transport of terrigenous sediment in the South Atlantic Ocean and their relations to glacial and interglacial cycles: Nd and Sr isotopic evidence. *Geochim. Cosmochim. Acta* **64,** 3813–3827.

Wehausen R. and Brumsack H.-J. (2000) Chemical cycles in the Pliocene sapropel-bearing and sapropel-barren eastern Mediterranean sediments. *Palaeoecol. Palaeoclimatol. Palaeoecol.* **158,** 325–352.

Weldeab S., Hemleben Ch., Emeis K.-C., and Siebel W. (2002) Provenance of lithogenic surface sediments and path ways of riverine suspended matters in the Eastern Mediterranean Sea: Evidence from $^{143}Nd/^{144}Nd$ and $^{87}Sr/^{86}Sr$ isotope ratios. *Chem. Geol.* **186,** 139–149.

Weldeab S., Emeis K.-C., Hemleben C., Schmiedl G., and Schulz H. (in press) Spatial productivity variations during formation of sapropel S5 and S6 in the Mediterranean Sea: Evidence from Ba contents. *Palaeogeogr. Palaeoclimatol. Palaeoecol.*

Wijmstra T. A., Young R., and Witte H. J. L. (1990) An evaluation of the climatic conditions during the Late Quaternary in northern Greece by means of multivariate analysis of palynological data and comparison with recent phytosociological and climatic data. *Geol. Mijnbouw* **69,** 243–251.

Yaalon D. H. and Ganor E. (1979) East Mediterranean trajectories of dust-carrying storms from the Sahara and Sinai. *Saharan Dust: Mobilization, Transport, Deposition, Scope* (ed. C. Morales), pp. 187–193. Wiley.